The Astrophysical Journal, 847:128 (10pp), 2017 October 1 https://doi.org/10.3847/1538-4357/aa88c8

Measuring the Growth Rate of Structure with Type IA Supernovae from LSST

Cullan Howlett[1,2], Aaron S. G. Robotham[1], Claudia D. P. Lagos[1,2], and Alex G. Kim[3]

[1] International Centre for Radio Astronomy Research, The University of Western Australia, Crawley, WA 6009, Australia; cullan.howlett@icrar.org

[2] ARC Centre of Excellence for All-sky Astrophysics (CAASTRO), Australia

[3] Lawrence Berkeley National Laboratory, 1 Cyclotron Road, Berkeley, CA 94720, USA

Received 2017 May 19; revised 2017 August 10; accepted 2017 August 25; published 2017 September 29

Abstract

We investigate the peculiar motions of galaxies up to $z = 0.5$ using Type Ia supernovae (SNe Ia) from the Large Synoptic Survey Telescope (LSST) and predict the subsequent constraints on the growth rate of structure. We consider two cases. Our first is based on measurements of the volumetric SNe Ia rate and assumes we can obtain spectroscopic redshifts and light curves for varying fractions of objects that are detected pre-peak luminosity by LSST (some of which may be obtained by LSST itself, and others that would require additional follow-up observations). We find that these measurements could produce growth rate constraints at $z < 0.5$ that significantly outperform those found using Redshift Space Distortions (RSD) with DESI or 4MOST, even though there are $\sim 4\times$ fewer objects. For our second case, we use semi-analytic simulations and a prescription for the SNe Ia rate as a function of stellar mass and star-formation rate to predict the number of LSST SNe IA whose host redshifts may already have been obtained with the Taipan+WALLABY surveys or with a future multi-object spectroscopic survey. We find ~18,000 and ~160,000 SNe Ia with host redshifts for these cases, respectively. While this is only a fraction of the total LSST-detected SNe Ia, they could be used to significantly augment and improve the growth rate constraints compared to only RSD. Ultimately, we find that combining LSST SNe Ia with large numbers of galaxy redshifts will provide the most powerful probe of large-scale gravity in the $z < 0.5$ regime over the coming decades.

Key words: cosmological parameters – cosmology: theory – large-scale structure of universe – supernovae: general

1. Introduction

A key science driver of future surveys such as DESI (Levi et al. 2013; DESI Collaboration et al. 2016) and 4MOST (de Jong et al. 2012) is to test general relativity (GR; Einstein 1916). While our consensus cosmological model (ΛCDM) has strong support from a variety of probes (Alam et al. 2017; Planck Collaboration et al. 2016; Riess et al. 2016; Hildebrandt et al. 2017), the nature of dark energy and matter remains unknown, and tensions exist between these results. Modifying the large-scale behavior of gravity is a promising alternative toward resolving this.

The peculiar velocities (PVs) of galaxies present a method to test gravity. The PV of a galaxy toward an overdensity at scale factor a is dictated by the growth rate of structure, $f(a) = d\ln D(a)/d\ln a$, which is the logarithmic derivative of the linear growth factor D. The linear growth factor in turn describes how density perturbations in the universe grow over cosmological time under the influence of gravity. Within the framework of ΛCDM and GR, the linear growth factor is given by (Heath 1977)

$$D(a) = \frac{5}{2}a^3\Omega_{m(a)}E^{3(a)}\int_0^a \frac{da'}{(a'E(a'))^3}, \quad (1)$$

where

$$\Omega_m(a) = \frac{\Omega_{m,0}}{a^3E^2(a)}, \quad (2)$$

$$E(a) = \sqrt{\frac{\Omega_{m,0}}{a^3} + \Omega_{\Lambda,0} + \frac{(1-\Omega_{m,0}-\Omega_{\Lambda,0})}{a^2}}, \quad (3)$$

and H_0, $\Omega_{m,0}$, and $\Omega_{\Lambda,0}$ describe the cosmological model. In turn, GR predicts a scale-independent growth rate that can be approximated as $f(a) \approx \Omega_m(a)^{0.55}$ (Linder & Cahn 2007). Measuring a growth rate that differs from this could be used to falsify GR and constrain alternative theories of gravity.

Redshift Space Distortions (RSD; Kaiser 1987) in the clustering of galaxies are the most commonly used method for constraining the growth rate, and the ability to make precise RSD measurements is an integral part of the design of DESI and 4MOST. However, this approach is fundamentally limited due to cosmic variance and the degeneracy between $f(a)$ and galaxy bias.

Direct measurements of PVs can instead be obtained by comparing the redshift-inferred distance to that measured using the intrinsic properties of the galaxy or its inhabitants. Examples include the Tully–Fisher (TF; Tully & Fisher 1977) and Fundamental Plane (FP; Djorgovski & Davis 1987; Dressler et al. 1987) relationships and the use of Type Ia supernovae (SNe Ia, Phillips 1993). These measurements are not affected by galaxy bias (Zheng et al. 2015), probe larger scales than the density field, and can be used to overcome the cosmic variance limit (Park 2000; Burkey & Taylor 2004). Koda et al. (2014) and Howlett et al. (2017a) showed that imminent redshift and PV surveys, such as Taipan (da Cunha et al. 2017) and WALLABY (Koribalski 2012), have the ability to produce some of the most accurate measurements of the growth rate to date.

In this work, we consider the capabilities of PVs measured using next generation measurements of SNe IA. Gordon et al. (2007), Bhattacharya et al. (2011), and Odderskov & Hannestad (2017) demonstrated that PVs obtained from the large number of SNe Ia we will detect with the Large Synoptic Survey Telescope (LSST) have the potential to constrain dark energy and the linear matter variance in spheres of radius 8 h^{-1} Mpc, σ_8. We instead build on the work of Howlett et al. (2017a) to show that, given host galaxy redshifts and accurate SNe classification, the two-point correlations between the velocities and positions of these

SNe Ia present a unique opportunity to measure the growth rate in the $z < 0.5$ universe. Using Fisher matrix forecasts, we find that these measurements could significantly improve the constraints found using just RSD with DESI and 4MOST.

Our aim is to present the constraints possible with SNe IA that will be detected (pre-peak luminosity) with LSST. However, LSST itself will only measure accurate light curves for a small percentage of these within its wide field survey. Additional follow-up observations will be needed to obtain host redshifts and spectroscopic classifications for all SNe IA, and improve on the overall photometric data quality and volume. Hence we provide forecasts for a variety of scenarios ranging from the typical numbers of SNe IA that may have accurate light curves from LSST itself, to the case where we can use additional follow-up to obtain light curves for all LSST detections. We then investigate the LSST-detected SNe IA we could expect to also have host redshifts from upcoming large galaxy surveys. Through this, we seek to motivate further consideration of the overlap between LSST and future spectroscopic surveys, the need for accurate photometric or spectroscopic follow-up of SNe IA whose light curves or types cannot be measured by LSST alone, and studies into how well PVs could be measured with SNe IA given realistic simulations of LSST.

Throughout, we quote AB magnitudes and assume a cosmology of $\Omega_m = 0.3121$, $\Omega_b = 0.0488$, $H_0 = 100\,h = 67.51$ km s^{-1} Mpc^{-1}, $n_s = 0.9653$, and $\sigma_8(z = 0) = 0.815$.

2. Peculiar Velocities with LSST SNe Ia

The LSST (Ivezic et al. 2008) project is a planned photometric survey whose large field of view and high cadence will allow for high-resolution imaging of approximately half the sky to be taken every few days. These properties will allow for the detections of millions of SNe Ia over the course of the survey. Measurements of the velocity field can be obtained from such a sample of SNe IA by taking the difference between the SNe Ia absolute magnitudes measured from their light curves and inferred from their apparent magnitudes and host galaxy redshifts (Johnson et al. 2014; Huterer et al. 2017). Equivalently, given a measurement of the distance modulus μ, and the host redshift z, we can define the "log-distance" ratio Δd, the logarithm of the ratio between the comoving distance inferred from the redshift d_z (in parsecs), and the true comoving distance,

$$\Delta d = \log_{10}\left(\frac{d_z}{10\ \mathrm{pc}}\right) - \frac{\mu}{5}. \quad (4)$$

The log-distance ratio can then be related to the PV using, for example, the estimator of Watkins & Feldman (2015)

$$v \approx \frac{cz_m}{1 + z_m}\ln(10)\Delta d, \quad (5)$$

where $z_m = z[1 + 1/2(1 - q_0)z - 1/6(1 - q_0 - 3q_0^2 + j_0)z^2]$ and q_0 and j_0 are the deceleration and jerk parameters. With the same sample of host galaxy redshifts we can also consider measurements of the density field and cross-correlations between the density and velocity fields.

In addition to the large numbers of measured PVs from LSST-detected SNe IA, the smaller intrinsic scatter in the SN Ia distance relationship compared to the TF or FP relations makes each one more useful for constraining gravity. We do not expect to be able to reduce the intrinsic scatter for TF or FP galaxies below 20% for even next generation surveys, but the distance error for SNe Ia is currently at the 10% level (Rest et al. 2014) and could be reduced to as little as 5% in the coming decades (Fakhouri et al. 2015). This allows us to probe the velocity field on larger scales and at higher redshifts than is currently possible. We focus on measurements of the two-point correlations between the density and velocity fields that will be obtainable with LSST SNe Ia, although other statistics, such as our local "bulk flow," could also be measured.

For all numbers in this work, we assume a 10-year LSST survey, and sky coverage of 18,000 deg^2. The LSST survey design we adopt for our forecasts is based on the LSST Observing Strategy White Paper (Marshall et al. 2017).[4] Simulations of the LSST observing strategy suggest ~40% of $z < 0.5$ SNe IA will be detected pre-peak luminosity and hence suitable for light-curve measurements. When discussing LSST-detected SNe IA, we are presenting numbers and forecasts weighted by this, i.e., we multiply the volumetric rate and SN IA rate as a function of stellar mass and star-formation rate (SFR) in the remainder of this work by 0.4.

3. LSST SNe Ia Numbers

3.1. Volumetric Rate

To predict the numbers of SNe Ia with PV measurements, we consider two different scenarios. First, we take a measurement of the volumetric rate of 6.8×10^{-5} $(1 + z)^{2.04}$ h^3 SN Ia yr^{-1} Mpc^{-3} (Dilday et al. 2010). For our adopted LSST survey, this gives a total of 120 SN Ia deg^{-2} up to $z = 0.5$ and $\sim 2.2 \times 10^6$ SN Ia in total. Of the SNe IA that LSST will detect, only a small fraction of those in the wide field survey will have enough repeat visits for accurate light curves to be measured. The latest simulations from the LSST Observing Strategy White Paper predict on the order of ~50,000 SN Ia yr^{-1} with accurate LSST light curves may be achievable for certain observing strategies. In the interest of motivating follow-up from other instruments, we consider forecasts for different numbers of LSST-detected SNe IA between those ~50,000 yr^{-1} that LSST may obtain distances for, up to the full number of ~220,000 yr^{-1}.

In all cases (including the following section), we assume that the LSST (and follow-up) observing strategy is designed so that the SNe IA with good light curves are randomly distributed within its wide footprint and that host redshifts and spectroscopic classifications can be obtained for these. In Section 5 we will discuss how the requirements for spectroscopic classification could be relaxed given accurate photometric typing, and the possible impact of systematic errors this could introduce. However, this is still an active area of research and the accuracy of photometric classifiers in the era of LSST is largely unknown, so for the purposes of our forecasts perfect classification is assumed. We will also investigate SN IA that may already have host redshifts from large galaxy surveys, which is logical to prioritize for follow-up. While obtaining light curves, host redshifts, and spectroscopic classifications for all LSST-detected SNe IA is optimistic, the number of galaxy

[4] This is a "living document," so more specifically, we use Version 0.99.d28199b found online at https://github.com/LSSTScienceCollaborations/ObservingStrategy/tree/master/whitepaper.

redshifts is far below the number of targets observable with next generation spectroscopic instruments and we expect nearly 100% of spectroscopic targets below $z = 0.2$ (which have the most accurate distances) to be "cheap" to obtain with a 1–2 m telescope.[5]

3.2. Pre-selected SNe Ia Hosts

For the second scenario, we consider LSST-detected SNe Ia for which host redshifts may have already been obtained by large spectroscopic galaxy surveys prior to or during LSST operations. These SNe Ia can be used in addition to the full spectroscopic galaxy sample to improve over the constraints from RSD alone. As such, these targets are the logical choice for additional follow-up if required, and many may already have LSST distance measurements. This is especially true considering, as we will show, the small number of SNe per year and the constraining power they offer when combined with the planned galaxy redshift surveys. In the following, we consider the combined Taipan (da Cunha et al. 2017) and WALLABY (Koribalski 2012) surveys, and a future spectroscopic sample with target density similar to DESI/4MOST.

To predict the number of SNe Ia, we combine a simulated galaxy catalog with observationally constrained models for the SNe Ia rate as a function of stellar mass and SFR. Our simulated catalog uses the Lagos et al. (2012) variant of the semi-analytic model GALFORM (Cole et al. 2000), which was run on merger trees constructed by Jiang et al. (2014) from the Millennium N-body simulation (Springel et al. 2005) and has an effective stellar mass limit of $10^8 M_\odot$. Lightcones of $z < 0.5$ and 1/16th full-sky area were constructed down to $r < 24.0$ using the algorithm described in Merson et al. (2013). Our additional selection functions are then applied on top of this. These lightcones reproduce the luminosity function and number counts of galaxies quite well from the near-UV to the IR (Gonzalez-Perez et al. 2014; Lagos et al. 2014; Lacey et al. 2016). Both semi-analytic models and hydrodynamical simulations typically give SFRs and colors that are up to 50% too low and 0.1 mag too blue, respectively (e.g., Lacey et al. 2016; Mitchell et al. 2016). We find that artificially increasing these in the simulation increases the number of SNe Ia by ~30%, which makes our forecasts conservative.

For the expected number of SNe Ia in these galaxies, we use Equation (5) from Smith et al. (2012). Figure 1 shows the number of LSST-detected SNe Ia and the total number of galaxies in our simulation as a function of stellar mass and specific SFR. As explained in Smith et al. (2012), large, late-type galaxies are the dominant source of SNe Ia. Massive, passive galaxies are relatively inefficient producers of low-redshift supernovae due to their old stellar populations, while the SFR tends to evolve slowly with redshift, such that galaxies with a high current SFR are likely to have had a high SFR in the past, giving rise to the majority of SNe Ia below $z = 0.5$.

The total number of $z < 0.5$ SNe Ia from the simulation, 29.3 SN Ia deg^{-2}, is a factor of ~4 lower than from the volumetric rate in Section 3.1. This discrepancy stems from the different methods for measuring the SNe Ia rate and inconsistencies between measurements of the SFR and stellar mass densities. For example, Smith et al. (2012) is consistent (depending on the exact model used) with Dilday et al. (2010) if one uses the measured densities of Hopkins & Beacom (2008) to convert between the two. They are not if we use the densities from our simulation or from more recent studies (S. P. Driver et. al. 2017, in preparation). However, these inconsistencies reduce the number of SNe Ia in the simulation relative to the volumetric rate (which is the simpler, and likely more robust measurement) and even in this case, we find that SNe Ia can be used to significantly augment the growth rate constraints from RSD alone.

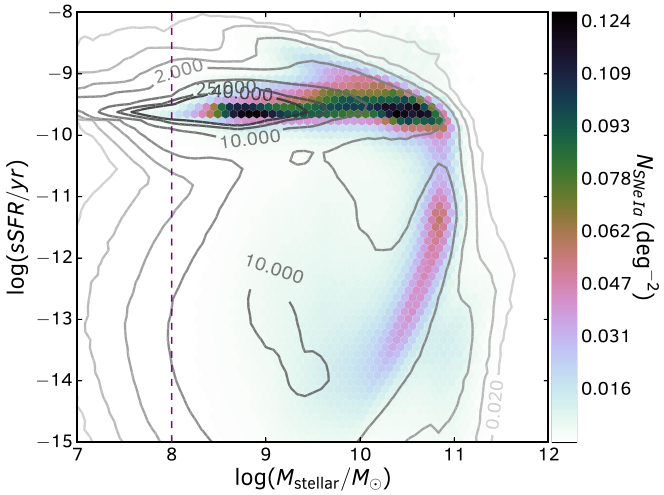

Figure 1. Numbers of SNe Ia (colored bins) and galaxies (gray contours) per deg^2 for our "pre-selected" scenario as a function of stellar mass and specific SFR. The vertical dashed line denotes the effective resolution limit within our simulation.

3.2.1. Taipan and WALLABY

We first consider the number of redshifts we could already have from the near-future Taipan and WALLABY surveys. Starting in 2017, the Taipan galaxy survey on the 1.2 m UK Schmidt Telescope will obtain optical spectra for over two million $z < 0.4$ galaxies across the southern sky ($\delta \lesssim 20$, $|b| \gtrsim 10$). The current design consists of a five year survey and uses 150 spectroscopic fibers (with a proposed upgrade to 300) spread across a 6° focal plane. The final data set will contain both a magnitude limited $i < 17.0$ sample and an LRG extension satisfying $17.0 < i < 18.1$ and $g - i > 1.6$, and this is the selection function we apply to our mock catalog. The sky coverage of Taipan overlaps almost fully with that of LSST and so we expect host redshifts to be already obtained for many SNe IA whose host galaxies satisfy either of these selection criteria. In addition to this, ~50,000 of the galaxies Taipan observes will have high enough signal to noise that they can be placed on the FP and used as distance indicators. Prior to the era of 4MOST/DESI and the opportunities presented with LSST-detected SNe IA, this will be the largest single PV survey, and of particular interest are those sources that will have both FP distances and PVs measured using SNe IA. Such a sample will allow for much greater control of systematics in the PV measurements from both SN Ia and the FP relationships.

Complementary to Taipan, the WALLABY survey (Koribalski 2012) is a planned 21 cm H I survey using the Australian SKA Pathfinder, which will cover three-quarters of the full-sky ($\delta < 30$) up to $z = 0.25$. Hence we expect full angular overlap between this survey and LSST. The survey uses newly designed

[5] For a comparison of current and future surveys, see http://compare.icrar.org/.

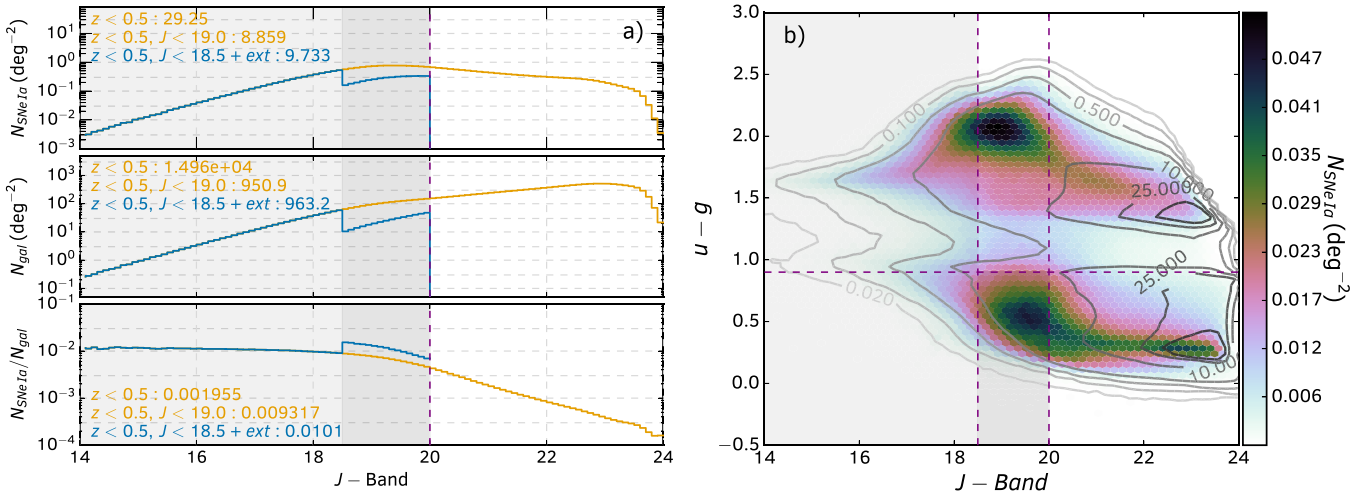

Figure 2. (a) Numbers of SNe Ia, galaxies and the efficiency of SN Ia production per deg^2 per bin of 0.1 dex for our "pre-selected" scenario as a function of J-band magnitude, for the full catalog (orange) and our ideal pre-selection (blue). We also give the total numbers for these selections. (b) Numbers of SNe Ia (colored bins) and galaxies (gray contours) as a function $u - g$ color and J-Band magnitude. In both cases shaded regions indicate the area we choose as our optimal selection: $J < 18.5$ plus an extension to $J < 20.0$ with $u - g < 0.9$.

phased array feeds with 30″ resolution over a frequency range of 1.13–1.43 GHz, while still allowing for a large 30 deg^2 field of view. The nomimal 1σ noise limit is expected to be 1.592 mJy km s^{-1} and in this work we consider all 5σ sources. WALLABY will be much more sensitive to low-redshift star-forming galaxies than Taipan (see Figure 11 in da Cunha et al. 2017), which due to their high SFR are still relatively efficient producers of SNe IA, and will measure redshifts to ∼500,000 galaxies, many of which will be missed by Taipan. As with Taipan, a significant fraction of these (∼30,000) are also expected to have PV measurements, this time determined via the TF relation, which will also be useful for reducing systematics.

From the selections for Taipan and WALLABY combined, we find 1.0 SN Ia deg^{-2} and ∼18,000 galaxies hosting LSST-detected SNe Ia, assuming a full overlap area of 18,000 deg^2. Even accounting for the factor of four difference between our volumetric rate based and simulation based predictions, this is only ∼7200 SNe IA per year of LSST operation and so well within the expected number that we could obtain with LSST alone, or with minimal follow-up.

3.2.2. A Future Multi-object Spectroscopic Survey

We then see how many hosts could be obtained from a future multi-object spectroscopic survey similar to DESI or 4MOST. These two multi-pass instruments will have ∼5000 and ∼1600 usable fibers, respectively, spread over 7.5 deg^2 and 4.1 deg^2 fields of view (de Jong et al. 2012; Levi et al. 2013). We do not tailor our selection to the requirements of any particular survey, but find that a high efficiency (ratio of the number of SNe Ia per target) is achieved with a selection close to that of the 4MOST Bright Galaxy (BG) sample. For a magnitude limited sample, J-band magnitudes allow for the highest efficiency; a $J < 19.0$ limit gives a target density of 951 deg^{-2}, 8.9 SN Ia deg^{-2}, and 0.9% of targets contain an LSST-detected SN Ia. We can slightly increase the efficiency using a $u - g$ color cut. A sample consisting of $J < 18.5$, plus an extension to $J < 20.0$ with $u - g < 0.9$ gives a similar target density, but increases the SNe Ia density to 9.7 SN Ia deg^{-2}. For comparison, observing the same target density but distributed randomly below $J < 20.0$ gives 7.1 SN Ia deg^{-2}, a decrease in efficiency of ∼30%. Overall, we predict ∼160,000 SN Ia detected by LSST, which could have host redshifts from a future $J < 19.0$ survey across 18,000 deg^2. Again, this number is small enough that a large fraction of such SNe IA could have light curves measured by LSST, although follow-up will likely be required to reach the full number, and we advocate prioritizing these targets that already have host galaxy redshifts.

Our two selections are summarized in Figure 2, where we plot the number of targets and SNe Ia per deg^2, and the efficiency as a function of J-band magnitude. We also show the $u - g$ color against J-band magnitude, highlighting the area we would preferentially target. Beyond our current selection the efficiency begins to fall significantly, hence obtaining additional host redshifts using dedicated programs may be preferable to a fainter pre-selection on planned large galaxy surveys.

The total number of galaxies and SN Ia as a function of redshift for all of our selections is shown in Figure 3. The Taipan and Wallaby surveys will measure many host redshifts for low-redshift SNe IA; however, this quickly drops off due to the sensitivity of these surveys. For a future multi-object spectroscopic survey, the number of SNe IA hosts we will obtain redshifts for remains high even up to $z = 0.5$, as the selections we consider mainly miss fainter or less star-forming galaxies, which are less efficient producers of SNe IA. These numbers of SNe IA are used as input for our forecasts in the following section.

Unfortunately, there is no current or planned photometry across the full southern hemisphere that could achieve our color selection. The current best option, the SkyMapper survey (Keller et al. 2007) will only go as faint as $u = 20.7$, $g = 21.7$. Including these constraints (and re-examining the other photometric bands under similar limits) shows that a complex selection would be required to improve beyond a simple $J < 19.0$ sample. Hence, this is the one we present in our forecasts.

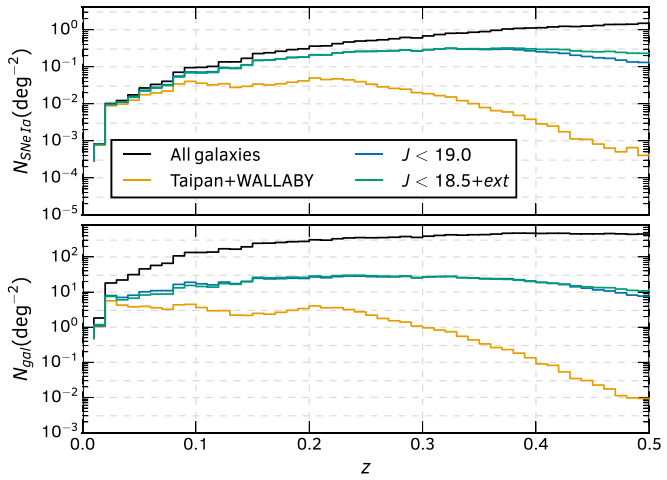

Figure 3. Numbers of SNe Ia and targets per deg^2 per $dz = 0.01$ bin for our "pre-selected" scenario as a function of redshift for all objects and for the three selections given in Section 3.2.

4. Fisher Matrix Forecasts on the Growth Rate

4.1. Method

We forecast the constraints on the growth rate using the Fisher matrix method of Howlett et al. (2017a), modeling the information contained in the two-point correlations between the density field measured using the galaxy redshifts and the velocity field from the SN Ia PVs. We have updated the Howlett et al. (2017a) models to account for the redshift dependence of the power spectra, growth rate, and galaxy bias, but otherwise the method remains unchanged. As such, we present only a brief overview here and we refer the reader to Howlett et al. (2017a) for a more complete description. The version of the code used to produce the growth rate forecasts in this paper is publicly available at https://github.com/CullanHowlett/PV_fisher.

For given parameters of interest $\boldsymbol{\lambda}$, we compute the corresponding elements of the Fisher Matrix $\mathbf{F}$, as

$$F_{ij} = \frac{\Omega_{\rm sky}}{4\pi^2}\int_{r_{\rm min}}^{r_{\rm max}} r^2 dr \int_{k_{\rm min}}^{k_{\rm max}} k^2 dk \int_0^1 d\mu_\phi \, \mathrm{Tr}\left[\mathbf{C}^{-1}(r,k,\mu_\phi)\frac{\partial \mathbf{C}(r,k,\mu_\phi)}{\partial \lambda_i}\mathbf{C}^{-1}(r,k,\mu_\phi)\frac{\partial \mathbf{C}(r,k,\mu_\phi)}{\partial \lambda_j}\right], \quad (6)$$

where $\Omega_{\rm sky}$ is the sky coverage of the survey, $r_{\rm max}$ ($r_{\rm min}$) are the comoving distances corresponding to the upper (lower) redshift limits of each redshift bin, and we set $k_{\rm max} = 0.2\,h$ Mpc^{-1} and $k_{\rm min} = 2\pi/r_{\rm max}$. μ_ϕ is the cosine of the angle ϕ between the k-vector and the observer's line of sight.

The covariance matrix, $\mathbf{C}$ consists of the anisotropic density–density, density–velocity, and velocity–velocity power spectra $P_{\delta\delta}$, $P_{\delta v}$, and P_{vv} respectively, as well as the noise associated with each of these,

$$\mathbf{C}(r,k,\mu_\phi) = \begin{bmatrix} P_{\delta\delta}(r,k,\mu_\phi) + \frac{1}{\bar{n}_\delta(r)} & P_{\delta v}(r,k,\mu_\phi) \\ P_{\delta v}(r,k,\mu_\phi) & P_{vv}(r,k,\mu_\phi) + \frac{\sigma^2_{\rm obs}(r)}{\bar{n}_v(r)} \end{bmatrix}. \quad (7)$$

The shot noise in these measurements is inversely proportional to the galaxy number density $\bar{n}_\delta(r)$ for the density field, and to the average PV error divided by the SN Ia number density $\sigma^2_{\rm obs}(r)/\bar{n}_v(r)$ for the velocity field. The average PV error is given in terms of a fractional distance error α, and a contribution from random motions $\sigma_{\rm obs,rand} = 300$ km s^{-1},

$$\sigma^2_{\rm obs}(r) = (\alpha H_0 r)^2 + \sigma^2_{\rm obs,rand}. \quad (8)$$

Finally, we model the relevant power spectra using

$$P_{\delta\delta}(z(r),k,\mu_\phi) = \left(\frac{1}{\beta^2(z)} + \frac{2\mu_\phi^2}{\beta(z)} + \mu_\phi^4\right)(f(z)\sigma_8(z))^2 D_g^2(k,\mu_\phi)\frac{P_{mm}(k,z)}{\sigma_8^2(z)}, \quad (9)$$

$$P_{\delta v}(z(r),k,\mu_\phi) = \frac{H(z)\mu_\phi}{k(1+z)}\left(\frac{1}{\beta(z)} + \mu_\phi^2\right)(f(z)\sigma_8(z))^2 D_g(k,\mu_\phi)D_u(k)\frac{P_{m\theta}(k,z)}{\sigma_8^2(z)}, \quad (10)$$

$$P_{vv}(z(r),k,\mu_\phi) = \frac{H^2(z)\mu_\phi^2}{k^2(1+z)^2}(f(z)\sigma_8(z))^2 D_u^2(k)\frac{P_{\theta\theta}(k,z)}{\sigma_8^2(z)}, \quad (11)$$

$$D_g(k,\mu_\phi) = \left[1 + \frac{(k\mu_\phi\sigma_\delta)^2}{2}\right]^{-1/2} \text{ and} \quad (12)$$

$$D_u(k) = \mathrm{sinc}(k\sigma_v). \quad (13)$$

We have written the above models in terms of the redshift corresponding to a given comoving distance $z(r)$ ($H(z)$ is the Hubble parameter at this redshift) and in a particular way to highlight the parameters of interest $\boldsymbol{\lambda} = \{f(z)\sigma_8(z), \beta(z), \sigma_\delta, \sigma_v\}$. The power spectra $P_{mm}(k,z)$, $P_{m\theta}(k,z)$, and $P_{\theta\theta}(k,z)$ are the real-space matter and velocity divergence auto- and cross-power spectra for the dark matter field and are computed using the implementation of two-loop Renormalized Perturbation Theory (Crocce & Scoccimarro 2006) found in the COPTER numerical package (Carlson et al. 2009).

The combination $f(z)\sigma_8(z)$ is the normalized growth rate that we present forecasts for in this work. We use this combination, as both f and σ_8 are degenerate on linear scales; however, their combination can still be used to constrain gravitational models even without explicit knowledge of σ_8 (Song & Percival 2009) and is what is typically measured using RSD and PV surveys. $\beta(z) = f(z)/b(z)$ is the ratio of the growth rate over the galaxy bias and here is treated as one of the nuisance parameters we marginalize over. We also marginalize over two additional nuisance parameters, σ_δ and σ_v, which characterize the nonlinear damping of the density and velocity fields due to RSD. These are used as inputs to Lorenztian (for the density field) and sinc (for the velocity field) functions, which reduce the power spectra on small scales but leave them unchanged on large scales. For these parameters we adopt the same values as used in Howlett et al. (2017a), $\sigma_\delta = 4.24\,h^{-1}$ Mpc and $\sigma_v = 13.0\,h^{-1}$ Mpc, which were found to reproduce the effects of nonlinear RSD in simulations (Koda et al. 2014).

Table 1
Forecasts for the Percentage Error on the Normalized Growth Rate $f\sigma_8$ for the RSD-only 4MOST-BG and DESI-BG Surveys and for Samples Containing LSST SNe Ia

Redshift	DESI-BGs[a]	4MOST-BGs[b]	All LSST-detected SNe Ia[c,d]		LSST Light Curves Only[c,e]		Taipan+WALLABY +SN Ia[c,f]	$J < 19.0$+SN Ia[c,g]
	RSD-only	RSD-only	RSD-only[h]	RSD+PVs	RSD-only[h]	RSD+PVs	RSD+PVs	RSD+PVs
$0.00 < z < 0.05$	56.8	57.1	66.3	20.1 (13.9)	106.6	41.0 (27.5)	25.4 (16.6)	24.3 (15.7)
$0.05 < z < 0.10$	21.5	21.6	24.6	11.5 (7.3)	38.5	22.7 (14.6)	15.9 (11.4)	14.6 (9.8)
$0.10 < z < 0.15$	13.2	13.2	14.8	9.0 (5.8)	22.6	16.6 (11.4)	11.8 (10.4)	10.6 (8.3)
$0.15 < z < 0.20$	9.6	9.7	10.6	7.5 (5.0)	15.8	13.0 (9.5)	9.1 (8.6)	8.2 (6.9)
$0.20 < z < 0.25$	7.7	7.6	8.3	6.3 (4.4)	12.1	10.5 (8.2)	7.4 (7.2)	6.7 (6.0)
$0.25 < z < 0.30$	6.5	6.4	6.8	5.5 (4.0)	9.8	8.8 (7.1)	7.2 (7.1)	5.7 (5.3)
$0.30 < z < 0.35$	5.8	5.5	5.8	4.9 (3.7)	8.2	7.6 (6.4)	8.3 (8.3)	5.0 (4.8)
$0.35 < z < 0.40$	5.5	5.0	5.1	4.4 (3.4)	7.1	6.7 (5.7)	13.9 (13.9)	4.5 (4.4)
$0.40 < z < 0.45$	5.9	4.8	4.6	4.1 (3.2)	6.3	6.0 (5.2)	…	4.2 (4.2)
$0.45 < z < 0.50$	10.9	5.8	4.2	3.8 (3.0)	5.7	5.4 (4.8)	…	4.1 (4.0)
$0.00 < z < 0.50$	**2.5**	**2.2**	**2.1**	**1.8 (1.3)**	**2.9**	**2.7 (2.2)**	**3.4 (3.2)**	**1.9 (1.7)**

Notes. The bold values are the constraints using information across the full redshift range.
[a] Using number densities from DESI Collaboration et al. (2016). Redshifts for all galaxies, no PVs.
[b] Using the number density of objects expected in the 4MOST-BG survey. Redshifts for all galaxies, no PVs.
[c] Assuming 10% (5%) distance errors.
[d] For all SNe IA detected by LSST as described in Section 3.1, assuming accurate light curves, redshifts, and PVs (from LSST or otherwise) from every SN IA.
[e] Assuming redshifts and PVs from only the ∼50,000 SN Ia yr^{-1}, detailed in Section 3.1, that could have accurate light curves from LSST alone.
[f] For the Taipan+WALLABY target selection in Section 3.2.1. Redshifts for all TAIPAN+WALLABY galaxies. PVs from the ∼18,000 SNe IA found in those galaxies.
[g] For the $J < 19.0$ selection in Section 3.2.2. Redshifts for all $J < 19.0$ galaxies. PVs from the ∼160,000 SNe IA found in those galaxies.
[h] Constraints when only the redshifts are used, regardless of available light-curve measurements.

The redshift dependence of the normalized growth rate and bias is included using $f(z)\sigma_8(z) = \Omega_m(z)^{0.55}\sigma_8(z=0)D(z)$ and $b(z) = b(z=0)D^{-1}(z)$, with $D(z)$ given by Equation (1) for $a = 1/(1+z)$ and normalized to unity at $z = 0$. Computing the necessary nonlinear real-space power spectra is slow, so the redshift dependence is captured by interpolating the power $P(k, z)$ at each k from a set of precomputed power spectra in the range of $z = [0.0, 0.5]$ with $\Delta z = 0.05$. We do not include any redshift dependence in σ_δ or σ_v.

We compute forecasts for the selections presented in Section 2; the volumetric rate with varying numbers of SNe IA with measured light curves and the number of SNe IA with host redshifts from Taipan, WALLABY, and a $J < 19.0$ survey. We compare these to the constraints using only RSD measured in the DESI-BG and 4MOST-BG surveys, i.e., where only the $P_{\delta\delta}(r, k, \mu_\phi)$ element of $\mathbf{C}(r, k, \mu_\phi)$ is non-zero. For all surveys, we assume a value for the galaxy bias $b(z=0) = 1.34$ to allow for a simpler comparison between results. The sky area for the SNe IA surveys is taken to be 18,000 deg^2, while we use 15,000 deg^2 for the RSD surveys, which closely matches the current design of 4MOST and DESI. For all SNe Ia samples, we consider distance errors of both 10% ($\alpha = 0.1$) and 5%.

We do not account for potential systematic errors in any of our forecasts; however, a discussion of how SN Ia systematics could affect measurements of the growth rate is given in Section 5.

4.2. Results

The percentage errors on the normalized growth rate, $f\sigma_8$ in bins of $\Delta z = 0.05$ between $z = 0.0$ and $z = 0.5$, and for the full redshift range, are listed in Table 1. The volumetric rate forecasts listed are those for the two limiting cases of only SNe IA that we expect to have light curves measured with LSST and for all LSST-detected SNe IA. For both of these we also give constraints from RSD only, i.e., the constraints using only the redshifts of the SNe IA to measure the density–density power spectrum, neglecting the additional information from their light curves. This shows the relative improvement when SNe IA PVs are added. For the SNe IA samples with pre-existing redshifts (last two columns), we emphasize that the constraints are from a combination of all the measured redshifts for these samples plus the much smaller number of SNe IA that add to the growth rate constraints from RSD alone.

We find similar constraints for the DESI-BG and 4MOST-BG surveys, reflecting their similar design and the fact that, as they only use RSD, these surveys quickly reach the cosmic variance limit at low redshift. The SNe Ia PVs allow us to break this limit as they sample the same underlying structure as the RSD measurements. This is most apparent at the lowest redshifts, where the volumetric rate predictions show a factor of ∼2 improvement over the RSD constraints, and where the $J < 19.0$ sample has significantly better constraints even though the selection function is similar to that of the 4MOST-BG sample.

The fractional errors for the RSD-only 4MOST-BG sample, all LSST-detected SNe Ia and our two samples where we only use SNe IA that are likely to already have host redshifts are plotted in Figure 4. The right-hand panel of this Figure then compares the LSST-detected SNe Ia constraints with and without SNe IA PVs against current measurements and the predictions from different models of gravity. For SNe Ia that are likely to already have host redshifts, the Taipan+WALLABY+SN Ia sample achieves better constraints than 4MOST or DESI below $z \approx 0.15$, but at higher redshifts the number of galaxies drops significantly resulting in poor constraining power. For the $J < 19.0$ sample the constraints are again comparable or better than with RSD-only for all redshift bins. This is because at low redshift the SNe Ia provide

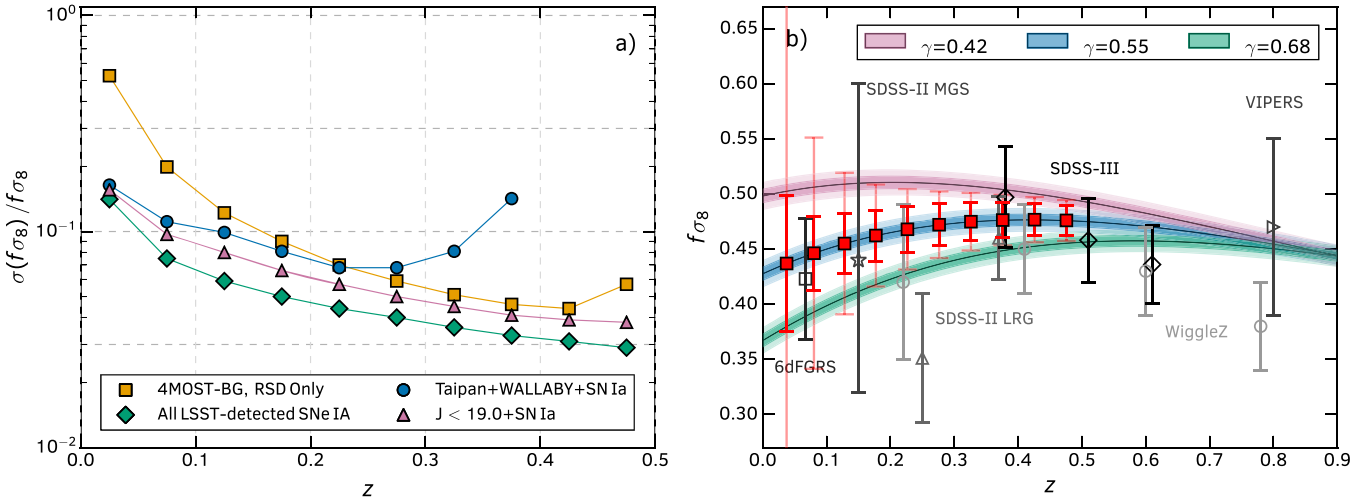

Figure 4. Forecasts for our three SNe Ia samples assuming 5% distance errors. (a) Fractional errors as a function of redshift plotted against the 4MOST-BG sample. (b) A comparison of the volumetric rate forecasts for all LSST-detected SNe IA (red squares) against existing measurements (Blake et al. 2011a, 2011b; Beutler et al. 2012; de la Torre et al. 2013; Oka et al. 2014; Howlett et al. 2015; Alam et al. 2017) and predictions from Planck (Planck Collaboration et al. 2016; normalized at the redshift of recombination) with different values for γ. These $f\sigma_8$ predictions as a function of redshift are calculated self-consistently using the method in Howlett et al. (2015) (Equations (26)–(30) therein), which accounts for the fact that the growth factor cannot be evaluated from Equation (1) for different values of γ. The outer error-bars for the volumetric rate measurements show RSD-only constraints (using only the redshift measurements of the SNe IA and neglecting their light curves); the inner show those including SNe Ia PVs. This highlights the redshift-dependent improvement due to the SNe Ia PVs.

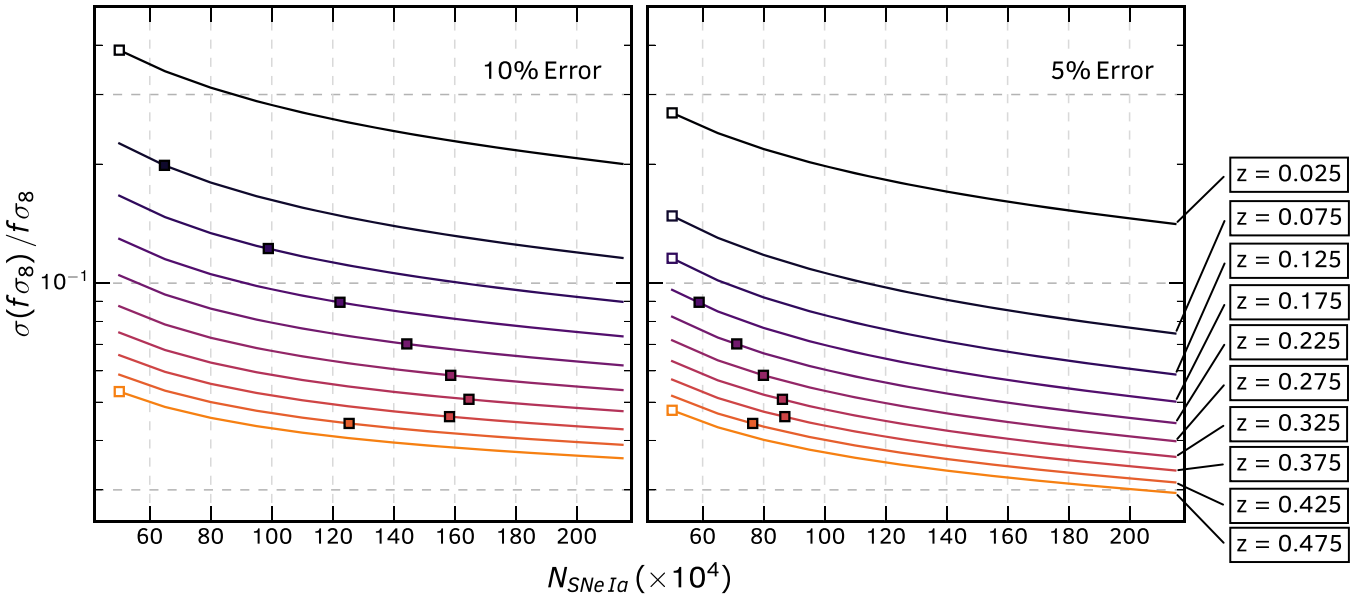

Figure 5. Forecasts for the fractional error on the growth rate as a function of SNe Ia with precise distance determinations, assuming distance errors of 10% (left) and 5% (right). Although survey-independent, the lower limit of the x-axis is equivalent to the SNe IA we expect to have light curves measured by LSST itself, while the upper limit is the expected number detected by LSST (for which distance measurements would require additional follow-up). Different lines represent different redshift bins of width $\Delta z = 0.05$. Points represent the intercept of each line with the RSD-only forecasts for the 4MOST-BG survey, and so allow us to infer the number of distance measurements necessary to improve over the 4MOST-BG constraints in each bin. Finally, open symbols represent cases where the light curves we expect from LSST alone already have greater predicted constraining power than 4MOST.

an increase in constraining power, while at high redshift we still obtain large numbers of galaxies and can constrain the growth rate via RSD, using the SNe Ia to break the degeneracy with any nuisance parameters.

In Figure 5, we demonstrate how the growth rate predictions change as we increase the number of SNe IA with distance measurements beyond those we are likely to obtain with LSST alone. We also plot the intersect of the fractional error as a function of the number of SNe IA in each redshift bin with the prediction using RSD from the 4MOST-BG sample. This intersect point highlights how many SNe IA with measured distances we would require in each redshift bin to improve over the constraint from 4MOST using RSD.

We find that, assuming 5% distance errors, the SNe IA distances we could obtain with LSST are already sufficient to improve over the RSD constraints below $z = 0.15$ and that measuring light curves to similar accuracy for only a modest fraction of the remaining LSST-detected SNe IA allows for superior constraints across the full redshift range we consider. For 10% distance errors, the required number of SNe IA is larger, but we can still improve on the 4MOST-BG constraints for all redshift bins using some fraction of the total number of

SNe IA LSST will detect. We emphasize here that, unlike our $J < 19.0$ predictions, the total number of objects (with SNe IA light curves and redshifts) even for all LSST detections is a factor of ∼4 less than the number of galaxies in the 4MOST or DESI-BG samples, which demonstrates the superior constraining power of the PV measurements.

We do not consider forecasts beyond $z = 0.5$ because at higher redshift the SNe Ia distance errors become large and the majority of the growth rate information comes from RSD (see Figure 4). While at $z = 0.5$, SNe Ia still help in marginalizing over the nuisance parameters, the constraining power of DESI and 4MOST improves significantly beyond this due to the large cosmological volumes they can probe with their Luminous Red Galaxy and Emission Line Galaxy samples. Combined, these can also be used to break the cosmic variance limit in the same way as a sample of SNe Ia. Hence the SNe Ia samples quickly become less competitive.

5. Systematics

In our analysis, we have assumed spectroscopic classification of the supernovae and have not included SN Ia systematics such as flux calibration or extinction correction errors, misclassification or the incorrect assignment of SN Ia to their host galaxies. The ability of photometric estimators to classify supernovae given LSST quality data and the magnitude of any systematic effects expected within LSST is currently under investigation but has not been clearly defined and so has not been included quantitatively in the forecasts we have presented. Here we provide a qualitative discussion of the need for spectroscopic classification and how we expect different systematic effects to manifest in measurements of the growth rate using the two-point correlations of the SNe IA PVs. A more rigorous analysis, measuring the velocity power spectrum using simulations of SNe IA as detected by LSST and including such systematic effects is left for future work.

5.1. SNe IA Measurement Systematics

Systematic errors within the flux calibration or extinction correction for a sample of SNe IA can be described via a limiting systematic "error floor" in each redshift bin or across the full SNe Ia sample (Linder & Huterer 2003; Kim & Linder 2011), such that for large numbers of SNe IA, the error on the mean distance measured in a given redshift bin does not continue to decrease purely in proportion to the square root of number of SNe IA. A systematic offset in the distance modulus resulting from this systematic error would act as an error on the zero-point of the SNe IA PVs, which is also present with other methods used to estimate PVs such as the TF and FP relations.

This is an issue for measurements of the bulk flow, where the zero-point acts in the same way as the bulk motion of the local universe, and a systematic error can bias bulk flow constraints. However, the velocity power spectrum is sensitive to the variance of the PVs as opposed to the mean, which is limited by the intrinsic dispersion in the distance indicator. In this way, Howlett et al. (2017a) showed that errors in the zero-point simply act as additional shot-noise in the velocity power spectrum and as long as the systematic errors are small compared to the intrinsic scatter, the effect of this on growth rate constraints is negligible. Alternatively, the additional shot-noise component can be marginalized over analytically and at little cost to the growth rate constraints (Johnson et al. 2014; Howlett et al. 2017b). In terms of quantities relevant to SNe IA, Linder & Huterer (2003) and Kim & Linder (2011) consider a systematic error in the distance modulus of around $\sigma_{\rm sys} \approx 0.03$ with some dependence on redshift. This is significantly less than even the lowest intrinsic dispersion we use in this work and might expect for future SNe IA, $\sigma_{\rm int} \approx 0.1$ and so we expect that the precision of the growth rate forecasts presented here will be unaffected by the inclusion of this systematic error.

5.2. Photometric Classification and Associated Systematics

Photometric classification of supernovae is an active area of study, with high-redshift supernova searches such as those in the Dark Energy Survey (The Dark Energy Survey Collaboration 2005) and LSST planning to perform photometric classification to define their cosmological samples (i.e., Campbell et al. 2013). However, current photometric classifiers, either template-based (e.g., Sako et al. 2011) or using machine learning (e.g., Lochner et al. 2016) are not perfect and introduce both systematic errors and potential biases into cosmological studies. A particularly subtle problem is that the very features useful for photometric classification: flux, color, light-curve shape, etc., are the same statistics used to determine supernova distances. This leads to strong covariance between an objects classification and distance measurement, whose impact in cosmological studies has yet to be studied in full. As the effects of these on LSST quality data and cosmological analyses in general is still not well understood, we have assumed for simplicity that we get spectroscopic redshifts of the host galaxies and classification of the supernova itself in our forecasts. This also negates the effects of SNe misclassification and host misidentifications. In the absence of spectroscopic classification, we would expect systematic errors due to both of these and discuss their expected impact on our forecasts below. Overall, the requirements for spectroscopic follow-up for measuring accurate SN Ia PVs may be relaxed, depending on progress in photometric classification over the coming years.

5.2.1. Misclassification

Misclassification of supernovae as SNe IA leads to contamination in the sample and incorrect distance inference. Photometric estimators typically also miss some fraction of true SNe IA. Accounting for completeness or false positives in the photometric classification of the SNe IA in our forecasts would reduce the total number of usable SNe IA, increase the shot-noise in our measurements of the velocity power spectrum, and reduce the constraints on the growth rate. However, the factor of 0.4 we have used in this work as the fraction of SNe IA LSST will detect pre-peak luminosity already carries considerable uncertainty, such that the effects of completeness on our growth rate forecasts are likely small compared to the current uncertainty in the factor of usable SNe IA we have assumed. Furthermore, we have provided forecasts assuming distance errors of both 5% and 10%, which can include contributions from both statistical and systematic errors. Even with the effects of misclassification of SNe, we consider distance errors of 10% to be conservative. Finally, it is worth noting that Type II-P SNe also show promise as "standardizable" candles (D'Andrea et al. 2010; de Jaeger et al. 2017) in the $z < 0.5$ universe, and are expected to be detected in even greater numbers with LSST than SNe IA (Ivezic et al. 2008). PVs from

such a sample have the potential to significantly improve over the forecasts presented here for SNe IA alone, even accounting for completeness and systematic errors.

5.2.2. Host Misidentification

While spectroscopic classification also provides a supernova redshift whose consistency can be tested with that of the purported host, the lack of that consistency test leads to misidentification of the host galaxy (Gupta et al. 2016). In the event that the true and assumed host galaxy are physically close, this is not an issue for PV measurements. In fact, a common practice is to use group galaxy catalogs measured from redshift surveys (i.e., Crook et al. 2007) to assign identical redshifts to PV targets belonging to the same group, which partially removes the effects of nonlinear motion on the measured PVs (Hong et al. 2014; Springob et al. 2014). In this sense, the SNe IA would be given the same observed redshift regardless of the host it is assigned to.

In the case of incorrect assignment of SNe IA to host galaxies that are close in angular separation but physically far apart, we expect to be able to remove these after the PVs have been measured. On linear scales, the PVs (excluding statistical errors) are expected to be Gaussian distributed. Hence, for physically distinct galaxies, the difference between the redshift distance and the true distance SNe IA measurements is likely to lead to an abnormally large PV, which can be then be removed via sigma-clipping, as was done for TF-based PVs in Howlett et al. (2017b).

6. Conclusions

We have demonstrated that LSST SNe Ia could provide measurements of the $z < 0.5$ growth rate that are more precise than those available using only RSD from DESI or 4MOST. Our best constraints come from the case where we are able to obtain host redshifts, light curves, and spectroscopic classification for all $\sim 2.2 \times 10^6$ LSST-detected SNe Ia, based on the volumetric SNe Ia rate from Dilday et al. (2010). There is currently no planned survey that can accomplish this; LSST is expected to obtain sufficiently accurate light curves for at most $\sim$500,000 of these; however, the target density, $\sim 12\ \mathrm{deg}^{-2}\ \mathrm{yr}^{-1}$, is small and could be accommodated as part of a larger survey program. We have also relaxed this condition and looked at how many SNe IA would be required to achieve constraints comparable to those from DESI or 4MOST at various redshifts, finding that SNe IA with light curves measured from LSST alone could do better than RSD below $z = 0.15$, given accurate classification and host redshifts. We expect many of these local SNe IA to already have host redshifts from upcoming galaxy redshift surveys.

To further explore this, we have combined simulated galaxy catalogs with a prescription for the SNe Ia rate as a function of stellar mass and SFR and explored those SNe Ia that could already have host redshifts from upcoming large galaxy surveys. Our test cases include Taipan, WALLABY, and a future multi-object spectroscopic survey. We find that a $J < 19.0$ magnitude limited sample could obtain $\sim$160,000 host redshifts. Although the number of SNe Ia is much smaller than the volumetric rate, predictions for the growth rate from this sample still outperforms those using only RSD with DESI or 4MOST. Hence, variations of the 4MOST or DESI target selections could allow for a large number of host redshifts that can be used to significantly augment and improve the constraining power of these surveys.

In this work, our primary aim is to motivate further consideration of the potential of LSST-detected SNe IA to measure the growth rate and test gravity. As such, we have assumed spectroscopic classification for our SNe and ignored potential systematic effects. This is also partly driven by our limited current understanding of both the ability of LSST quality photometry to overcome these effects and the covariance and bias introduced into measurements of SNe IA distances when using photometric classification methods. We have discussed how we expect various measurement systematics to manifest in measurements of the growth rate and anticipate that the assumption of spectroscopic classification can be relaxed as photometric estimators progress. Future studies will allow us to quantify the effects of various systematics and classification algorithms on the velocity power spectrum we will measure with LSST SNe IA, and this work motivates a careful study of these in the context of testing gravity.

We thank Bob Nichol, Eric Linder, Patrick McDonald, David Parkinson, and Chris Blake for their comments and the latter for providing the number density of the 4MOST-BG sample. This research was conducted by the Australian Research Council Centre of Excellence for All-sky Astrophysics (CAASTRO), through project number CE110001020. This research has made use of NASA's Astrophysics Data System Bibliographic Services and the `astro-ph` pre-print archive at https://arxiv.org/. All plots in this paper were made using MATPLOTLIB (Hunter 2007).

ORCID iDs

Aaron S. G. Robotham https://orcid.org/0000-0003-0429-3579

References

Alam, S., Ata, M., Bailey, S., et al. 2017, MNRAS, 470, 2617A
Beutler, F., Blake, C., Colless, M., et al. 2012, MNRAS, 423, 3430
Bhattacharya, S., Kosowsky, A., Newman, J. A., & Zentner, A. R. 2011, PhRvD, 83, 043004
Blake, C., Brough, S., Colless, M., et al. 2011a, MNRAS, 415, 2876
Blake, C., Glazebrook, K., Davis, T. M., et al. 2011b, MNRAS, 418, 1725
Burkey, D., & Taylor, A. N. 2004, MNRAS, 347, 255
Campbell, H., D'Andrea, C. B., Nichol, R. C., et al. 2013, ApJ, 763, 88
Carlson, J., White, M., & Padmanabhan, N. 2009, PhRvD, 80, 043531
Cole, S., Lacey, C. G., Baugh, C. M., & Frenk, C. S. 2000, MNRAS, 319, 168
Crocce, M., & Scoccimarro, R. 2006, PhRvD, 73, 063519
Crook, A. C., Huchra, J. P., Martimbeau, N., et al. 2007, ApJ, 655, 790
da Cunha, E., Hopkins, A. M., Colless, M., et al. 2017, PASA, submitted (arXiv:1706.01246)
D'Andrea, C. B., Sako, M., Dilday, B., et al. 2010, ApJ, 708, 661
de Jaeger, T., González-Gaitán, S., Hamuy, M., et al. 2017, ApJ, 835, 166
de Jong, R. S., Bellido-Tirado, O., Chiappini, C., et al. 2012, Proc. SPIE, 8446, 84460T
de la Torre, S., Guzzo, L., Peacock, J. A., et al. 2013, A&A, 557, A54
DESI Collaboration, Aghamousa, A., Aguilar, J., et al. 2016, arXiv:1611.00036
Dilday, B., Smith, M., Bassett, B., et al. 2010, ApJ, 713, 1026
Djorgovski, S., & Davis, M. 1987, ApJ, 313, 59
Dressler, A., Lynden-Bell, D., Burstein, D., et al. 1987, ApJ, 313, 42
Einstein, A. 1916, AnP, 354, 769
Fakhouri, H. K., Boone, K., Aldering, G., et al. 2015, ApJ, 815, 58
Gonzalez-Perez, V., Lacey, C. G., Baugh, C. M., et al. 2014, MNRAS, 439, 264
Gordon, C., Land, K., & Slosar, A. 2007, PhRvL, 99, 081301
Gupta, R. R., Kuhlmann, S., Kovacs, E., et al. 2016, AJ, 152, 154

Heath, D. J. 1977, MNRAS, 179, 351
Hildebrandt, H., Viola, M., Heymans, C., et al. 2017, MNRAS, 465, 1454
Hong, T., Springob, C. M., Staveley-Smith, L., et al. 2014, MNRAS, 445, 402
Hopkins, A. M., & Beacom, J. F. 2008, ApJ, 682, 1486
Howlett, C., Ross, A. J., Samushia, L., Percival, W. J., & Manera, M. 2015, MNRAS, 449, 848
Howlett, C., Staveley-Smith, L., & Blake, C. 2017a, MNRAS, 464, 2517
Howlett, C., Staveley-Smith, L., Elahi, P. J., et al. 2017b, MNRAS, 471, 3135
Hunter, J. D. 2007, CSE, 9, 90
Huterer, D., Shafer, D. L., Scolnic, D., & Schmidt, F. 2017, JCAP, 5, 015
Ivezic, Z., Tyson, J. A., Abel, B., et al. 2008, arXiv:0805.2366
Jiang, L., Helly, J. C., Cole, S., & Frenk, C. S. 2014, MNRAS, 440, 2115
Johnson, A., Blake, C., Koda, J., et al. 2014, MNRAS, 444, 3926
Kaiser, N. 1987, MNRAS, 227, 1
Keller, S. C., Schmidt, B. P., Bessell, M. S., et al. 2007, PASA, 24, 1
Kim, A. G., & Linder, E. V. 2011, JCAP, 6, 020
Koda, J., Blake, C., Davis, T., et al. 2014, MNRAS, 445, 4267
Koribalski, B. S. 2012, PASA, 29, 359
Lacey, C. G., Baugh, C. M., Frenk, C. S., et al. 2016, MNRAS, 462, 3854
Lagos, C. D. P., Baugh, C. M., Zwaan, M. A., et al. 2014, MNRAS, 440, 920
Lagos, C. d. P., Bayet, E., Baugh, C. M., et al. 2012, MNRAS, 426, 2142
Levi, M., Bebek, C., Beers, T., et al. 2013, arXiv:1308.0847
Linder, E. V., & Cahn, R. N. 2007, APh, 28, 481
Linder, E. V., & Huterer, D. 2003, PhRvD, 67, 081303
Lochner, M., McEwen, J. D., Peiris, H. V., Lahav, O., & Winter, M. K. 2016, ApJS, 225, 31
Marshall, P., Anguita, T., Bianco, F. B., et al. 2017, arXiv:1708.04058
Merson, A. I., Baugh, C. M., Helly, J. C., et al. 2013, MNRAS, 429, 556
Mitchell, P. D., Lacey, C. G., Baugh, C. M., & Cole, S. 2016, MNRAS, 456, 1459
Odderskov, I., & Hannestad, S. 2017, JCAP, 1, 060
Oka, A., Saito, S., Nishimichi, T., Taruya, A., & Yamamoto, K. 2014, MNRAS, 439, 2515
Park, C. 2000, MNRAS, 319, 573
Phillips, M. M. 1993, ApJL, 413, L105
Planck Collaboration, Ade, P. A. R., Aghanim, N., et al. 2016, A&A, 594, A13
Rest, A., Scolnic, D., Foley, R. J., et al. 2014, ApJ, 795, 44
Riess, A. G., Macri, L. M., Hoffmann, S. L., et al. 2016, ApJ, 826, 56
Sako, M., Bassett, B., Connolly, B., et al. 2011, ApJ, 738, 162
Smith, M., Nichol, R. C., Dilday, B., et al. 2012, ApJ, 755, 61
Song, Y.-S., & Percival, W. J. 2009, JCAP, 10, 004
Springel, V., White, S. D. M., Jenkins, A., et al. 2005, Natur, 435, 629
Springob, C. M., Magoulas, C., Colless, M., et al. 2014, MNRAS, 445, 2677
The Dark Energy Survey Collaboration 2005, arXiv:astro-ph/0510346
Tully, R. B., & Fisher, J. R. 1977, A&A, 54, 661
Watkins, R., & Feldman, H. A. 2015, MNRAS, 450, 1868
Zheng, Y., Zhang, P., & Jing, Y. 2015, PhRvD, 91, 123512